AGU PUBLICATIONS

Geophysical Research Letters

RESEARCH LETTER
10.1002/2016GL071153

Key Points:
- Preexplosive magmatic conduit was reconstructed from pumice analysis
- Conduit was filled up to ~10 km depth with gas-saturated magma
- The magma had enough gas to sustain the high-energy explosion

Supporting Information:
- Supporting Information S1

Correspondence to:
A. Burgisser,
alain.burgisser@univ-savoie.fr

Citation:
Drignon, M. J., T. Bechon, L. Arbaret, A. Burgisser, J.-C. Komorowski, C. Martel, H. Miller, and R. Yaputra (2016), Preexplosive conduit conditions during the 2010 eruption of Merapi volcano (Java, Indonesia), *Geophys. Res. Lett.*, *43*, 11,595–11,602, doi:10.1002/2016GL071153.

Received 8 SEP 2016
Accepted 31 OCT 2016
Accepted article online 3 NOV 2016
Published online 22 NOV 2016

Preexplosive conduit conditions during the 2010 eruption of Merapi volcano (Java, Indonesia)

Mélissa J. Drignon[1], Tonin Bechon[2,3], Laurent Arbaret[2,3], Alain Burgisser[4], Jean-Christophe Komorowski[5], Caroline Martel[2,3], Hayden Miller[6], and Radit Yaputra[7]

[1]College of Earth, Ocean, and Atmospheric Sciences, Oregon State University, Corvallis, Oregon, USA, [2]Université d'Orléans, ISTO, Orléans, France, [3]CNRS, ISTO, Orléans, France, [4]Université Savoie Mont Blanc, CNRS-INSU, ISTerre, Le Bourget du Lac, France, [5]Institut de Physique du Globe de Paris, Sorbonne Paris Cité, Université Paris Diderot, Paris, France, [6]Division of Geological and Planetary Sciences, Caltech, Pasadena, California, USA, [7]Pusat Vulkanologi dan Mitigasi Bencana Geologi, CVGHM, Yogyjakarta, Indonesia

Abstract The 2010 eruption is the largest explosive event at Merapi volcano since 1872. The high energy of the initial 26 October explosions cannot be explained by simple gravitational collapse, and the paroxysmal explosions were preceded by the growth of a lava dome not large enough to ensure significant pressurization of the system. We sampled pumice from these explosive phases and determined the preexplosive depths of the pumices by combining textural analyses with glass water content measurements. Our results indicate that the magma expelled was tapped from depths of several kilometers. Such depths are much greater than those involved in the pre-2010 effusive activity. We propose that the water-rich magma liberated enough gas to sustain the explosivity. Our results imply that the explosive potential of volcanoes having dome-forming, effusive activity is linked to the depth from which fresh magma can be evacuated in a single explosion, regardless of the evacuated volume.

1. Introduction

Effusive activity producing viscous lava domes that collapse due to gravity is by far the most common recent eruptive mode of Merapi volcano, Indonesia [*Siswowidjoyo et al.*, 1995; *Voight et al.*, 2000; *Ratdomopurbo et al.*, 2013]. This pattern of activity was disrupted in 2010 by the largest explosive eruption since 1872, which led to the evacuation of about 0.5 million people [*Surono et al.*, 2012]. This unusual event occurred in several stages between 26 October and 23 November 2010 [*Komorowski et al.*, 2013; *Jenkins et al.*, 2013]. Precursory signs were observed during the preceding year, with outgassing and ash emissions, and increased seismicity during the month leading to the crisis. The first large explosion occurred on 26 October 2010, lasted 2 h and produced a 12 km high ash plume and pyroclastic flows that reached 7.5 km away from the summit [*Surono et al.*, 2012; *Charbonnier et al.*, 2013]. It had a phreatomagmatic component that has been interpreted as a laterally directed explosion from a gas-rich stalled intrusion or newly formed cryptodome [*Komorowski et al.*, 2013; *Jousset et al.*, 2013]. This event was fed by the collapsing 2006 lava dome, parts of the older summit dome complex, and a minor component of juvenile 2010 magma. After a succession of lava domes that collapsed gravitationally over the next few days, the paroxysmal stage of the 2010 eruption started on 5 November. Several Vulcanian blasts were immediately followed by a subplinian convective fountain collapse [*Komorowski et al.*, 2013]. Finally, low-level ash emission and outgassing (release of gases trapped in the magma as bubbles) occurred until the end of eruptive activity.

This unusual crisis has left behind a series of puzzling observations; the explanations of which would improve our understanding of the processes governing such a dramatic change in eruptive intensity. One observation is that the high energy of the 26 October pyroclastic density currents cannot be explained by simple gravitational collapse of the mostly degassed 2006 dome and cold summit rocks [*Cronin et al.*, 2013]. This led to the hypothesis that the minor amount of 2010 magma involved in this event was responsible for its highly explosive nature [*Surono et al.*, 2012]. The involvement of large amounts of carbonates and CO_2 was at first evoked as a possible cause of the 2010 explosivity [*Deegan et al.*, 2010; *Borisova et al.*, 2013], but recent petrologic evidences concur that the role of carbonates was not abnormal [*Costa et al.*, 2013; *Erdmann et al.*, 2016]. The cryptodome created degassing conditions that seem similar to those of the previous domes, which suggests that the upper part of the conduit did not sustain unusually high overpressure [*Kushnir et al.*, 2016].

Remarkably high ascent rates are additional observations that set the 2010 eruption apart [*Costa et al*., 2013; *Preece et al*., 2014; *Pallister et al*., 2013].

Here we show that only a small volume of the new, 2010 magma was necessary to generate the high-energy 26 October explosion because it was unusually volatile rich due to its deep origin compared to previous events that were dominated by dome and shallow juvenile material. We sampled pumices from the explosive phases of 26 October and 5 November. We determined the preexplosive depths of the pumices by combining textural analyses with glass water content measurements. We measured the oxygen isotopic composition of selected samples to test whether sample rehydration between eruption and sampling has occurred. Water contents were converted to pressures by using a physical model of recompression [*Burgisser et al*., 2010] and to depths by using the method of *Burgisser et al*. [2011]. Our results give a preexplosive image of the volatile distribution within the conduit prior to the opening and paroxysmal stages of the 2010 eruption.

2. Material and Methods

Sampling of the dense, amphibole-bearing pyroxene andesites followed the stratigraphy defined by *Komorowski et al*. [2013] (Text S1 in the supporting information). Forty-one samples from the 26 October pyroclastic density current deposits and 13 samples from the 5 November pyroclastic density current and air fall deposits were prepared for analyses. Small cores ~2 cm^3 were drilled in each pumice. In six cases, two cores were taken from the same large clasts from 26 October to quantify natural variability at the centimeter scale. The half of the core closest to the clast surface was discarded so as to avoid weathering effects, while the other half was cut in two, one being subjected to textural analysis and the other being used for H_2O measurement. This procedure ensured that the various analyses characterize the same volume of sample.

The oxygen isotopic composition ($\delta^{18}O$) of 13 samples was measured by laser fluorination at Caltech following a procedure derived from *Sharp* [1990] and *Valley et al*. [1995]. Briefly, 2–3 mg of bulk pumice is irradiated by a 20 μm laser in the presence of BrF_5 vapor, driving fluorination reactions that produce O_2, HF, and other fluorinated species. The O_2 is isolated and purified by cryogenic separation and passaging through hot mercury, then converted to CO_2 by passaging over hot graphite and analyzed in this form by dual-inlet gas source mass spectrometry. This procedure maximizes precision (0.4‰) while minimizing sample size.

The textural characterization of the samples was done by two methods. Thirty-six samples were characterized by scanning electron microscope (SEM). Polished sections were imaged using a TESCAN MIRA 3 XMU SEM operating at 20 to 25 kV accelerating voltage (CNRS-ISTO, Université d'Orléans) in backscattered electron mode. Images were used to manually quantify in each sample the amounts of phenocrysts, microlite, vesicles, and glass following *Giachetti et al*. [2010]. Sixteen other samples were characterized by element mapping by energy-dispersive spectroscopy (EDS probe EDAX PEGASUS attached to the SEM) to automate the textural analysis and to better quantify the mineral phases present. The remaining 21 samples were characterized by associating them to textural groups that were defined by optical microscopy observations and that had at least one sample analyzed by EDS (Text S2).

In samples analyzed by SEM, vesicles were subdivided in three categories using the criteria of *Giachetti et al*. [2010]. Large, deformed vesicles of equivalent diameter >300 μm and circularity <0.2 were deemed preexplosive vesicles. Small, rounded vesicles of equivalent diameter <40 μm and circularity >0.65 were deemed synexplosive, isolated vesicles. Finally, the rest of the vesicles were deemed synexplosive, connected vesicles. This categorization leaves aside angular, large void spaces between crystal fragments. These were observed in only one sample, and they accounted for less than 10% of the total vesicularity.

Weight fractions of glass, ${}^jX_{gl}$, neglect the weight of the vesicles and were calculated differently whether the textural analysis was conducted by SEM or by EDS because each method characterized objects of differing nature (Text S2):

$$ {}^jX_{gl} = \frac{X_{\text{bulk}}\,\Sigma_i {}^jV_i\rho_i - X_a R\, {}^1V_{a+cpx}\,\rho_a}{{}^jV_{gl}\rho_{gl}} \tag{1} $$

where j is an index characterizing the analysis type (0 for SEM and 1 for EDS), X_{bulk} is the bulk H_2O weight

fraction, $X_a = 0.02$ is the H_2O weight fraction in amphibole, $R = 0.25$ is the assumed constant ratio between the volume fraction of amphibole and that of amphibole plus clinopyroxene [*Erdmann et al*., 2016], and ρ are the densities (amphibole density $\rho_a = 3300\,kg/m^3$). When the textural analysis was conducted by SEM, $j = 0$; ${}^1V_{a+cpx} = 0$; and $\sum_i {}^jV_i\rho_i = {}^0V_{\mu l}\rho_{\mu l} + {}^0V_{\mu p}\rho_{\mu p} + {}^0V_{gl}\rho_{gl} + {}^0V_{ox}\rho_{ox}$, where V are the volume fractions and the subscripts gl, μl, μp, and ox, respectively, mean glass, microlite, microphenocryst, and oxides ($\rho_{\mu l} = \rho_{\mu p} = 2570$, $\rho_{gl} = 2380$, and $\rho_{ox} = 4720\,kg/m^3$). When the textural analysis was conducted by EDS, $j = 1$ and $\sum_i {}^jV_i\rho_i = {}^1V_{opx}\rho_{opx} + {}^1V_{a+cpx}\rho_{a+cpx} + {}^1V_{gl}\rho_{gl} + {}^1V_{ox}\rho_{ox} + {}^1V_{ca}\rho_{ca} + {}^1V_{plag}\rho_{plag}$, where the subscripts opx, $a+cpx$, Ca, and $plag$, respectively, mean orthopyroxene, amphibole + clinopyroxene, Ca-dominated minerals (apatite and Ca-bearing xenoliths), and plagioclase ($\rho_{opx} = \rho_{a+cpx} = 3300$, $\rho_{Ca} = 2700$, and $\rho_{plag} = 2570\,kg/m^3$). Uncertainties on X_{gl} were calculated by error propagation (Text S2).

We used the Flash 2000 elemental analyzer (ISTO, Université d'Orléans), which yields total H contents in 10 min per sample. Samples were crushed with an agate mortar, while visible (>200 μm) phenocrysts (method A) or large (>0.8 mm) amphiboles and pyroxenes (method B) were removed by hand to obtain ~7 mg of powder <30 μm. Method A was used with the samples analyzed by SEM, and 200 μm corresponds to the limit below which a human eye cannot easily distinguish a crystal from a piece of interstitial glass. The faster method B was used for samples analyzed by EDS and optical microscope. All powder samples were deposited in tin capsules and placed in a furnace at 900°C. They were heated to ~1800°C in the presence of O_2, and a helium flux transported the liberated H in H_2O form. Water was dissociated from other volatiles by chromatography and analyzed by thermal conductivity. We used the certified standard SOIL (LECO, H = 0.41 wt %), but its value had to be recalibrated for the silicate rocks analyzed herein to H = 0.339 wt % by using a combination of the standards PYRO (5% H_2O by Karl Fisher titration (KFT)) and SULFA (Thermo, H = 4.68 wt %). This recalibration was tested by reproducing water contents of volcanic glasses previously measured by KFT (e.g., sample AMO42 of *Burgisser et al*. [2010]). Total amounts of H given by the elemental analyzer were converted to bulk H_2O content using H and O molar masses. Each sample was analyzed several times in order to reduce measurement error. Samples analyzed 3 times or more have a relative error on X_{bulk} that is the largest and lies between that of the sample series and that of the standard that was analyzed at regular intervals during a measurement day. The relative error of the daily standard series was attributed to samples analyzed twice.

Two physical models were used to convert variables measured in the pumice to preexplosive conditions. The first model uses vesicularities from the textural analyses and interstitial glass water contents to estimate preexplosive pressures and porosities [*Burgisser et al*., 2010]. It has four free parameters (two related to bubble populations, one related to the quench pressure, and one related to outgassing; Text S3), which were combined to yield 11 sets of preexplosive pressures and porosities. The set with the reference values (see below) of the free parameters was kept as the average set, and the two sets with the largest and smallest porosity values at any pressure were kept as extremes characterizing model uncertainty. Analytical uncertainties for each sample were calculated with an additional four sets of outputs that used the average values of the free parameters and the respective minimum and maximum values of glass water content and vesicularity.

Preexplosive pressures were converted into preexplosive depths following *Burgisser et al*. [2011]. Briefly, each sample is assumed to represent a slice of the magma column, and the slice thickness is adjusted so that the pressure at its base due to the overlying load equals that determined using water contents. Only two end-member scenarios were used. The first assumes that pressure is magmastatic, i.e., that the pressure in the magma column is created by the sole weight of magma because conduit walls are fully rigid. In the second scenario pressure is lithostatic, which implies that the conduit walls are not rigid.

3. Results

Results from the laser fluorination analyses are given in Figure 1 and Table S1 in the supporting information. Samples from both eruptive stages, 26 October and 5 November, gave results from $\delta^{18}O = 4.970 \pm 0.036‰$ for the densest sample, AME10F-a, to $\delta^{18}O = 6.402 \pm 0.014‰$ for a moderately vesicular sample, AME10B-a. This is much lower than sedimentary carbonates at Merapi, $\delta^{18}O > 19‰$, and in the low range of the 2010 products, $5.6 < \delta^{18}O < 7‰$ [*Troll et al*., 2013].

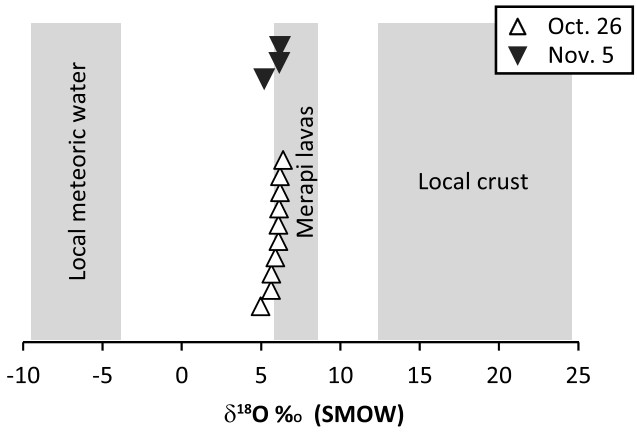

Figure 1. Oxygen isotopic composition of bulk samples of the 2010 Merapi eruption. The open triangles are 26 October samples, and the closed triangles are 5 November samples (*y* axis corresponds to $\delta^{18}O$ relative sorting order). Values are relative to the standard mean ocean water (SMOW) composition. Local meteoric waters are from *Cobb et al.* [2007]. Local crust comprises volcanoclastics and limestone, and Merapi lavas are whole-rock analyses [*Troll et al.*, 2013].

The 48 samples from the 26 October event have 30–60 vol % phenocrysts on a vesicle-free basis, except AME10F1 which has 20 vol % phenocrysts (Tables S2–S4). Microlite proportions range from 16 to 42 vol %, except AME10B4, which has 50 vol % microlites. Vesicle-free glass contents range from 12 to 70 vol %. Bulk vesicularities range from 11 to 57 vol %, and glass water contents range from 0.10 ± 0.09 to 6.6 ± 1.9 wt %. Isolated synexplosive vesicles, connected synexplosive vesicles, and connected preexplosive vesicles are present in respective proportions of 2.5 ± 1.4:69.1 ± 7.0:28.4.

On a vesicle-free basis, the 14 samples from the 5 November event have 30–60 vol % phenocrysts, 8–33 vol % microlite, and 22–67 vol % glass. Bulk vesicularities range from 16 to 61 vol %, and glass water contents range from 0.55 ± 0.08 to 1.6 ± 0.4 wt %. Isolated synexplosive vesicles, connected synexplosive vesicles, and connected preexplosive vesicles are present in respective proportions of 1.6 ± 0.9:69.6 ± 8.1:28.8. All these values are broadly similar to those from the 26 October samples, except for the lower range of glass water content.

Considering all 2010 samples together, there is no correlation between glass water content and vesicularity (Figure S3 in the supporting information) and a broad positive correlation between glass water content and microlite content (Figure S4).

In using the model to estimate preexplosive pressures and porosities [*Burgisser et al.*, 2010] (a user-friendly version of the model is available as an MS Excel spreadsheet; see Acknowledgments section), a magma temperature of 950°C and a bubble-free magma density of 2455 kg/m^3 (i.e., melt + crystals) are assumed [*Costa et al.*, 2013]. The two free parameters linked to bubble populations were constrained by the proportions of the three vesicle types and their uncertainties. Following *Burgisser et al.* [2010], the parameter constraining the amount of overpressure that clasts can sustain was set to the reference value of $1^{-0.5}_{+1}$. The upper and lower values of the last parameter, which quantifies outgassing, were chosen so that the maximum total water content is <7.6 wt % and that all clasts had net synexplosive inflation, as suggested by textural observations. The former condition takes into account the maximum glass water content measured in our samples and yields a water saturation pressure of 315 MPa, which is a reasonable upper value for the magma storage region where most of the crystallization occurs [*Preece et al.*, 2014]. These conditions imply that between 10 and 82% of the gas present synexplosively were outgassed, with an assumed reference value of 50% for this poorly constrained parameter that has a modest effect on preexplosive pressures.

Figure 2a shows the preexplosive pressures as a function of the preexplosive porosities. Clasts from the 26 October event originate from pressures spanning a remarkable wide range, from nearly atmospheric to ~250 MPa with porosities confined between 0.5 and 20 vol %. The number of samples is large enough to give a representative pressure-porosity distribution. Giving a precise upper preexplosive pressure limit, however, is difficult. The five samples with the largest pressures have large (~30%) uncertainties on X_{gl}. Grouping these five samples, the maximum melt H_2O content is 6.0 ± 1.9 wt %, which corresponds to a maximum pressure of 230 ± 100 MPa. Clasts from the 5 November event have pressures from ~6 to ~90 MPa and porosities from 1.5 to 20 vol %. The smaller number of analyzed clasts is not representative enough to prove that the magma involved into the paroxysmal stage of the eruption comes exclusively from a shallower part of the conduit than that of the opening explosive stage of 26 October. Overall, preexplosive melt water contents are slightly (3 to 15%) higher than glass water contents at quench time (Table S3).

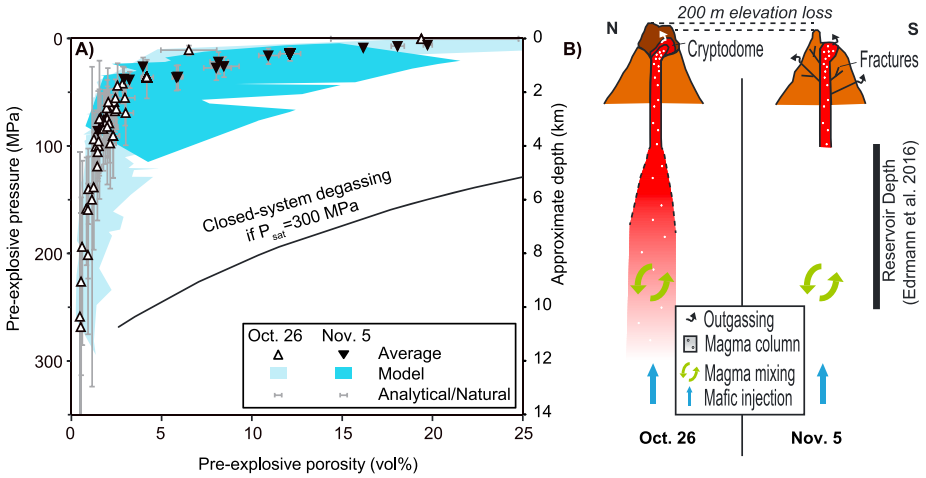

Figure 2. Preexplosive magmatic columns represented as porosity as a function of pressure and depth. (a) The triangles indicate the average model output for the two eruptive stages (open for 26 October and closed for 5 November). The blue areas cover the ranges of outputs of the 10 parametric model runs (light blue for 26 October and dark blue for 5 November). The error bars represent the combined effects of natural variability and analytical uncertainty on each sample. The solid black curve indicates the closed-system degassing if the pure water saturation pressure is 300 MPa. (b) Schematic representation of the conduit prior to each explosive event.

Uncertainties on the porosities are dominated by model assumptions, whereas uncertainties in preexplosive pressures reflect the natural variability of glass content in the samples. Comparing the glass contents in sample pairs issued from the same clast shows that the glass content varies within one clast by up to 13 vol %, which supports the latter assertion (Table S2). Taking all these uncertainties into account, it is statistically significant that the 5 November samples follow the trend of the 26 October samples.

The right vertical axis of Figure 2a shows approximate preexplosive depths of the two 2010 events. These are estimated thanks to two scenarios of overpressure in the conduit (Figure S5). No overpressure corresponds to a magmastatic pressure distribution, and some overpressure is conferred by assuming elastic conduit walls that reestablish a lithostatic pressure. There are only small differences between these two scenarios because of the low preexplosive porosities, so a single depth axis with an intrinsic uncertainty of ±5% is used in Figure 2 to illustrate that the 26 October magmatic column was evacuated to ~10 km deep.

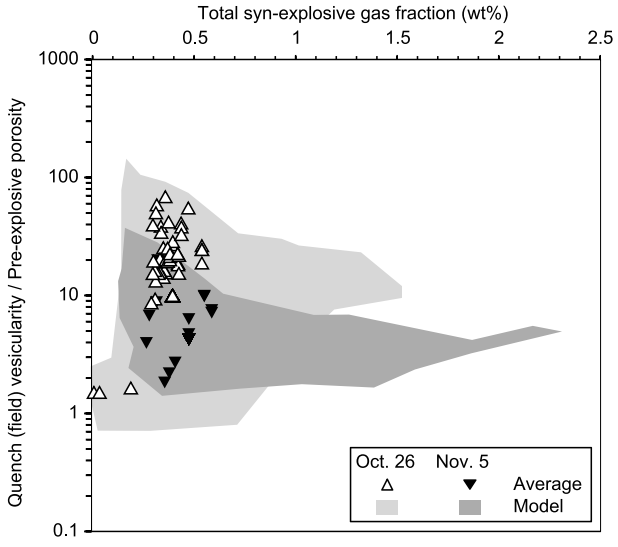

Figure 3. Total synexplosive gas fraction as a function of the ratio of bulk vesicularity and preexplosive porosity. The triangles indicate the average model output for the two eruptive stages (open for 26 October and closed for 5 November). The gray areas cover the ranges of outputs of the 10 parametric model runs (light gray for 26 October and dark gray for 5 November).

Figure 3 shows the ratio of bulk vesicularity over preexplosive porosity as a function of total gas amount at quench time (gas in the bubbles plus the outgassed fraction). The porosity ratio is a measure of the amount of synexplosive expansion, and the total gas amount quantifies the maximum amount of gas that was involved in propelling the explosion. The minimum amount of propelling gas is given by taking only the fraction outgassed, which is half the total gas fraction for the reference values shown on Figure 3. The 26 October clasts have expanded by up to a factor of 70 and

released 0.3–0.5 wt % gas during the explosion. As expected, pumices ejected on 5 November have expanded far less than those of 26 October but produced a similar amount of propelling gas.

4. Discussion

We sampled pumices from the 2010 Merapi eruption 3 years after the event. *Giachetti and Gonnermann* [2013] suggested that sample rehydration between eruption and sampling may occur, which would lead to an overestimation of the preexplosive pressures. There are several lines of evidence that it is not the case. First, there is no relationship between water content and porosity in our samples (Figure S3) [*Giachetti and Gonnermann*, 2013]. Second, rehydration of rhyolitic glass is only 10^{-3}–10^{-4} μm^2/yr [*Liritzis and Laskaris*, 2011; *Seligman et al*., 2016]. The short time between eruption and sampling and our use of drilled cores of pumice make it improbable that our samples were affected by meteoric water. Third, our measures of $\delta^{18}O$ from bulk pumice match *Troll et al*.'s [2013] values for Merapi phenocrysts, which agree with expected values of $\delta^{18}O = +5‰$ to $+6‰$ for igneous rocks [*Eiler et al*., 2000]. Finally, our water contents agree with that of the low-vesicularity pumice of *Genareau et al*. [2014] and with total H_2O amounts reported by *Borisova et al*. [2013] for the 2010 products.

Our analysis neglects CO_2, the presence of which may affect our preexplosive pressure estimates. Measuring CO_2 in the 2010 products has been shown to be difficult. Glass CO_2 values obtained by *Genareau et al*. [2014] on 2010 pumices are far above the solubility limit for conditions compatible with that eruption. These authors interpret such values, which cannot represent the CO_2 dissolved in the melt, as being caused by residual carbonate material from assimilation. As a result, our preexplosive pressures are minimum values. A modification of the *Burgisser et al*. [2010] model to take CO_2 into account using an estimate of the CO_2/H_2O molar ratio in the fluid phase from *Erdmann et al*. [2016] indicates that our preexplosive pressures are underestimated by an amount at most comparable to measurement uncertainties (Text S4). This is consistent with physical considerations (conduit collapse and the presence of a magmatic reservoir), suggesting that it is unlikely that the conduit was evacuated over depths much greater than the 10 km we calculate (Figure 2b). This implies that the pumices from the 26 October event were H_2O rich and CO_2 poor, as suggested by experimental petrology [*Erdmann et al*., 2016].

The deep origin of the clasts explains the explosivity of the 26 October event despite the low amount of juvenile material (~5 vol % assuming that juvenile components were concentrated in the surge deposits [*Cronin et al*., 2013]). Taking only the juvenile component, 0.3 to 0.5 wt % H_2O was mobilized synexplosively as a gas that underwent a 10–70-fold volume expansion. The effect of the amount of volatile and originating depth can be illustrated by assuming that the 26 October samples had only 1/10 of the glass water content we measured. This hypothetical magma column would be restricted to pressures <10 MPa with <0.5 wt % gaseous H_2O that would volumetrically expand at most twofold.

Similarly to the 5 November event at Merapi, Vulcanian explosions at Soufrière Hills (Montserrat) in 1997 and at Mount St. Helens (U.S.) in July 1980 were inferred to evacuate the shallow (<4 km) parts of the conduit [*Cashman and McConnell*, 2005; *Diller et al*., 2006; *Platz et al*., 2007; *Burgisser et al*., 2010, 2011]. This reinforces the hypothesis that the controls of the transition between Plinian-style, dynamic magma ascent and Vulcanian-style, static unloading of conduit are less linked to shallow conduit dynamics than to the dynamics of the underlying magma reservoir.

Our data are helpful to better understand the 2010 Merapi eruption. Before 26 October, the summit was capped by the remaining dome from the 2006 eruption. A new magma rose from >14 km, generating volcanotectonic earthquakes and changes in fumarole activity a month before eruption [*Surono et al*., 2012; *Budi-Santoso et al*., 2013], and summit deformation and seismicity associated to cryptodome formation and outgassing days before the eruption [*Surono et al*., 2012; *Jousset et al*., 2013]. These time frames (a month for new magma emplacement and days for cryptodome formation) were sufficient for the new magma to significantly outgas and reduce its porosity to <20 vol % (Figure 2b). The fact that gas release as measured by SO_2 flux [*Surono et al*., 2012] did not increase markedly before the peak flux of 26 October suggests that the magma column had stalled. Our sampling is representative of the full length of the conduit, which suggests that the gas was mostly able to escape from the magma, but it is insufficient at low pressures (<30 MPa) to determine whether this gas was volumetrically small and/or was stored at shallow levels, possibly in the cryptodome.

Our sampling of the 5 November event shows that the magma column that caused the paroxysmal phase of the eruption had similar characteristics to that feeding the 26 October event. Before 5 November, the volcano summit had been reduced by 200 m [*Jousset et al*., 2013] and explosions pulverized successive, newly formed small domes [*Komorowski et al*., 2013]. The country rock was probably damaged, allowing the substantial outgassing that our data and the 5×10^5 t/d sulfur emissions recorded between 4 and 5 November [*Surono et al*., 2012] suggest. Our data also support the interpretation that the dome that grew prior to the main explosion was probably not large enough to maintain a fully closed system and associated large overpressure [*Komorowski et al*., 2013; *Kushnir et al*., 2016].

Gas escape from the magma through a permeable network of bubbles, or outgassing, is one of the reasons why andesitic volcanoes switch from an explosive phase to an effusive one. Our results suggest that the 2010 Merapi magma was extensively outgassed, yielding a dense magma column just prior to the beginning of the 2010 crisis. This implies that the driving force behind this event was not so much the amount of gas present in the conduit than the availability in the volcanic conduit of magma rich in dissolved water. The state of the magmatic column had thus changed in nature from the previous eruptive cycle (2006 to possibly as early as 1878 [*Voight et al*., 2000]) to allow magma tapping to great depths. The 2010 crisis thus appears as a rapid succession of conduit filling and emptying with insufficient feeding from below to trigger a larger Plinian eruption. The 2013 shallow explosion, which remobilized some of the 2010 dome [*Walter et al*., 2015], suggests that a small fraction of magma prone to be easily evacuated is still present in the shallow magmatic system. If no water-rich magma recharges the deeper system and ascends rapidly, however, it is likely that the pre-2010, mostly effusive regime, will prevail during the next eruptive phase.

5. Conclusions

Our results show that a very small volume of fresh magma (<10%) was sufficient to sustain the high-energy pyroclastic density currents and associated ash plume of the first explosive stage of the Merapi 2010 eruption on 26 October because its deep origin allowed it to be unusually rich in dissolved water. The preexplosive magmatic conduit was filled from depth to near the summit with water-rich magma that liberated enough gas to sustain the explosivity of the event. This magma had sufficient time to rise from the magmatic reservoir(s) to be significantly outgassed, leaving a dense magma that fed the explosive event. A similar reconstruction of the preexplosive conduit conditions of the 5 November paroxysmal stage corroborates that the magma expelled during this eruption was tapped from depths of several kilometers, unlike the most common, pre-2010, effusive activity. Our results imply that the explosive potential of volcanoes having dome-forming, effusive activity is linked to the depth from which fresh magma can be transported by a single explosion, regardless of the erupted volume.

Acknowledgments

We would like to thank N. Cholik and S. Sumarti of the Merapi Volcano Observatory (CVGHM) in Yogyakarta for their help with fieldwork. We are grateful to S. Cox, M. Lloyd, S. Newman, and J. Eiler for their assistance at the Caltech Isotope Lab; to L. Moulin and N. Perard for their work on the EDS methodology; to I. Di Carlo for her help at the SEM in Orléans; and to S. Erdmann for providing the amphibole compositions. Useful reviews by T. Giachetti and J. Pallister were appreciated. This work was partially funded by the ANR DoMerapi (ANR-12-BS06-0012) and by a grant from Labex OSUG@2020 (Investissements d'avenir—ANR10 LABX56). The data used are available at https://isterre.fr/annuaire/pages-web-du-personnel/alain-burgisser/article/softwares?lang=fr.

References

Borisova, A.Y., C. Martel, S. Gouy, I. Pratomo, S. Sumarti, J.-P. Toutain, I.N. Bindeman, P. de Parseval, J.-P. Metaxian, and J.-P. Surono (2013), Highly explosive 2010 Merapi eruption: Evidence for shallow-level crustal assimilation and hybrid fluid, *J. Volcanol. Geotherm. Res.*, *261*, 193–208.

Budi-Santoso, A., P. Lesage, S. Dwiyono, S. Sumarti, S. Subandriyo, P. Jousset, and J.-P. Metaxian (2013), Analysis of the seismic activity associated with the 2010 eruption of Merapi volcano, Java, *J. Volcanol. Geotherm. Res.*, *261*, 153–170.

Burgisser, A., S. Poussineau, L. Arbaret, T. H. Druitt, T. Giachetti, and J.-L. Bourdier (2010), Pre-explosive conduit conditions of the 1997 Vulcanian explosions at Soufrière Hills Volcano, Montserrat: I. Pressure and vesicularity distribution, *J. Volcanol. Geotherm. Res.*, *194*, 27–41.

Burgisser, A., L. Arbaret, T. H. Druitt, and T. Giachetti (2011), Pre-explosive conduit conditions of the 1997 Vulcanian explosions at Soufrière Hills Volcano, Montserrat: II. Overpressure and depth distributions, *J. Volcanol. Geotherm. Res.*, *199*, 193–205.

Cashman, K. V., and S. M. McConnell (2005), Multiple levels of magma storage during the 1980 summer eruptions of Mount St. Helens, WA, *Bull. Volcanol.*, *68*, 57–75.

Charbonnier, S. J., A. Germa, C. B. Connor, R. Gertisser, K. Preece, J.-C. Komorowski, F. Lavigne, T. Dixon, and L. Connor (2013), Evaluation of the impact of the 2010 pyroclastic density currents at Merapi volcano from high-resolution satellite imagery, field investigations and numerical simulations, *J. Volcanol. Geotherm. Res.*, *261*, 295–315.

Cobb, K. M., J. F. Adkins, J. W. Partin, and B. Clark (2007), Regional-scale climate influences on temporal variations of rainwater and cave dripwater oxygen isotopes in northern Borneo, *Earth Planet. Sci. Lett.*, *263*, 207–220.

Costa, F., S. Andreastuti, C. Bouvet de Maisonneuve, and J. S. Pallister (2013), Petrological insights into the storage conditions, and magmatic processes that yielded the centennial 2010 Merapi explosive eruption, *J. Volcanol. Geotherm. Res.*, *261*, 209–235.

Cronin, S. J., G. Lube, D. S. Dayudi, S. Sumarti, S. Subrandiyo, and Surono (2013), Insights into the October–November 2010 Gunung Merapi eruption (central Java, Indonesia) from the stratigraphy, volume and characteristics of its pyroclastic deposits, *J. Volcanol. Geotherm. Res.*, *261*, 244–259.

Deegan, F. M., V. R. Troll, C. Freda, V. Misiti, J. P. Chadwick, C. L. McLeod, and J. P. Davidson (2010), Magma-Carbonate Interaction Processes and Associated CO2 Release at Merapi Volcano, Indonesia: Insights from Experimental Petrology, *J. Petrol.*, *51*(5), 1027–1051, doi:10.1093/petrology/egq010.

Diller, K., A. B. Clarke, B. Voight, and A. Neri (2006), Mechanisms of conduit plug formation: Implications for Vulcanian explosions, *Geophys. Res. Lett.*, *33*, L20302, doi:10.1029/2006GL027391.

Eiler, J. M., A. Crawford, T. Elliott, K. A. Farley, J. W. Valley, and E. M. Stolper (2000), Oxygen isotope geochemistry of oceanic arc lavas, *J. Petrol.*, *41*, 229–256.

Erdmann, S., C. Martel, M. Pichavant, J.-L. Bourdier, R. Champallier, J.-C. Komorowski, and N. Cholik (2016), Constraints from phase equilibrium experiments on pre-eruptive storage conditions in mixed magma systems: A case study on crystal-rich basaltic andesites from Mount Merapi, Indonesia, *J. Petrol.*, *57*(3), 535–560, doi:10.1093/petrology/egw019.

Genareau, K., S. J. Cronin, and G. Lube (2014), Effects of volatile behaviour on dome collapse and resultant pyroclastic surge dynamics: Gunung Merapi 2010 eruption, in *The Role of Volatiles in the Genesis, Evolution and Eruption of Arc Magmas*, *Special Publications* 410, edited by G. F. Zellmer et al. doi:10.1144/SP410.6, Geol. Soc., London.

Giachetti, T., T. H. Druitt, A. Burgisser, L. Arbaret, and C. Galven (2010), Bubble nucleation, growth and coalescence during the 1997 Vulcanian explosions of Soufrière Hills volcano, Montserrat, *J. Volcanol. Geotherm. Res.*, *193*, 215–231.

Giachetti, T. M., and H. M. Gonnermann (2013), Water in volcanic pyroclast: Rehydration or incomplete degassing?, *Earth Planet. Sci. Lett.*, *369–370*, 317–332.

Jenkins, S., J.-C. Komorowski, P. Baxter, R. Spence, A. Picquout, F. Lavigne, and Surono (2013), The Merapi 2010 eruption: An interdisciplinary impact assessment methodology for studying pyroclastic density current dynamics, *J. Volcanol. Geotherm. Res.*, *261*, 316–329.

Jousset, P., A. Budi-Santoso, A. D. Jolly, M. Boichu, S. Surono, S. Dwiyono, P. H. Sumarti, and S. Thierry (2013), Signs of magma ascent in LP and VLP seismic events and link to degassing: An example from the 2010 explosive eruption at Merapi volcano, Indonesia, *J. Volcanol. Geotherm. Res.*, *261*, 171–192.

Komorowski, J.-C., S. Jenkins, P. T. Baxter, A. Picquout, F. Lavigne, S. Charbonnier, R. Gertisser, N. Cholik, A. Budi-Santoso, and Surono (2013), Paroxysmal dome explosion during the Merapi 2010 eruption: Processes and facies relationships of associated high-energy pyroclastic density currents, *J. Volcanol. Geotherm. Res.*, *261*, 260–294.

Kushnir, A. R. L., C. Martel, J.-L. Bourdier, M. J. Heap, T. Reuschle, S. Erdmann, J.-C. Komorowski, and N. Cholik (2016), Probing permeability and microtexture: Unravelling the role of a low-permeability dome on the explosivity of Merapi (Indonesia), *J. Volcanol. Geotherm. Res.*, *316*, 56–71.

Liritzis, I., and N. Laskaris (2011), Fifty years of obsidian hydration dating in archeology, *J. Non-Cryst. Solids*, *357*, 2011–2023.

Pallister, J. S., D. J. Schneider, J. P. Griswold, R. H. Keeler, W. C. Burton, C. Noyles, C. G. Newhall, and A. Ratdomopurbo (2013), Merapi 2010 eruption—Chronology and extrusion rates monitored with satellite radar and used in eruption forecasting, *J. Volcanol. Geotherm. Res.*, *261*, 144–152, doi:10.1016/j.jvolgeores.2012.07.012.

Platz, T., S. J. Cronin, K. V. Cashman, R. B. Stewart, and I. E. M. Smith (2007), Transition from effusive to explosive phases in andesite eruptions—A case-study from the AD 1655 eruption of Mt. Taranaki, New Zealand, *J. Volcanol. Geotherm. Res.*, *161*, 15–34.

Preece, K., R. Gertisser, J. Barclay, K. Berlo, R. A. Herd, and E. I. M. Facility (2014), Pre- and syn-eruptive degassing and crystallisation processes of the 2010 and 2006 eruptions of Merapi volcano, Indonesia, *Contrib. Mineral. Petrol.*, *168*, 1061, doi:10.1007/s00410-014-1061-z.

Ratdomopurbo, A., F. Beauducel, J. Subandriyo, I. G. M. Agung Nandaka, C. G. Newhall, Suharna, D. S. Sayudi, H. Suparwaka, and Sunarta (2013), Overview of the 2006 eruption of Mt. Merapi, *J. Volcanol. Geotherm. Res.*, *261*, 87–97, doi:10.1016/j.jvolgeores.2013.03.019.

Seligman, A. N., I. N. Bindeman, J. M. Watkins, and A. M. Ross (2016), Water in volcanic glass: From volcanic degassing to secondary hydration, *Geochim. Cosmochim. Acta*, *191*, 216–238.

Sharp, Z. D. (1990), A laser-based microanalytical method for the in situ determination of oxygen isotope ratios of silicates and oxides, *Geochim. Cosmochim. Acta*, *54*, 1353–1357.

Siswowidjoyo, S., I. Suryo, and I. Yokoyama (1995), Magma eruption rates of Merapi volcano, central Java, Indonesia during one century (1890–1992), *Bull. Volcanol.*, *57*, 111–116.

Surono, P., et al. (2012), The 2010 explosive eruption of Java's Merapi volcano—A "100-year" event, *J. Volcanol. Geotherm. Res.*, *241–242*, 121–135.

Troll, V. R., et al. (2013), Magmatic differentiation processes at Merapi volcano: Inclusion petrology and oxygen isotopes, *J. Volcanol. Geotherm. Res.*, *261*, 38–49.

Valley, J. W., N. Kitchen, M. J. Kohn, C. R. Niendorf, and M. J. Spicuzza (1995), UWG-2, a garnet standard for oxygen isotope ratios: Strategies for high precision and accuracy with laser heating, *Geochim. Cosmochim. Acta*, *59*, 5223–5231.

Voight, B., E. K. Constantine, S. Siswowidjoyo, and R. Torley (2000), Historical eruptions of Merapi volcano, central Java, Indonesia, 1768–1998, *J. Volcanol. Geotherm. Res.*, *100*, 69–138.

Walter, T. R., J. Subandriyo, S. Kirbani, H. Bathke, W. Suryanto, N. Aisyah, H. Darmawan, P. Jousset, B.-G. Luehr, and T. Dahm (2015), Volcano-tectonic control of Merapi's lava dome splitting: The November 2013 fracture observed from high resolution TerraSAR-X data, *Tectonophysics*, *639*, 23–33.